BES Analysis Memo

Observation of a narrow $p\bar{p}$ state in $J/\psi \to \gamma p\bar{p}$ decays

Stephen L. Olsen and Daniela Paluselli

(January 15, 2002)

Abstract

We report the observation of a narrow structure with mass near $2m_p$ in the $p\bar{p}$ mass spectrum produced in the radiative decay process $J/\psi \to \gamma p\bar{p}$. The results are based on a 17.8 pb^{-1} data sample that contains 50 million J/ψ decays. The absence of any evidence for this structure in a 6.0 pb^{-1} data sample accumulated at the $\psi(2S)$ resonance is used to establish that the observed state is produced by J/ψ decays and is not due to a radiative return process.

I. INTRODUCTION

In this memo, we report the observation of a narrow, resonance-like structure with mass near $2m_p$ in the $p\bar{p}$ system produced in the radiative decay process $J/\psi \to \gamma p\bar{p}$. Earlier versions of this analysis were described in memos posted in March, September and October 2001. This note supersedes and replaces those reports. Additional supporting information is available on the web [1].

The analysis is based on the entire BES-II 50 million J/ψ event sample. As a calibration process, we identify the process $J/\psi \to \gamma\eta_C$; $\eta_C \to p\bar{p}$. We also report results of a search for this state in the BES-I sample of 4×10^6 $\psi(2S)$ events. The absence of any evidence for this state in the $\psi(2S)$ sample provides evidence that the state is produced in J/ψ decays and not in a radiative return process.

II. EVENT SELECTION

We use events with at least two oppositely charged tracks and at least one neutral track with $E_{BSC} > 0.05$ GeV, all in the polar angle region $|\cos\theta| < 0.8$. We assign the highest momentum positively (negatively) charged track as the proton (antiproton) candidate and veto events where *both* candidate tracks are identified as muons or where *both* tracks have associated BSC showers with $E > 0.8$ GeV. At least one of the charged tracks is required to have a proton probability greater than 0.05. Neutral and charged track parameters are corrected with the versions of NCOR.F and SUPERFUG.F sent out by Xiaoyan on 8/24/01.

The surviving events are subjected to 4-C fits to the hypotheses $J/\psi \to K^+K^-\gamma$ and $J/\psi \to p\overline{p}\gamma$. If there are more than one candidate γ, the γ that produces the lowest χ^2 to the $J/\psi \to p\overline{p}\gamma$ hypothesis is selected. Also, events with more than one γ are subjected to a 5-C fit to the hypothesis $J/\psi \to p\overline{p}\pi^0$; $\pi^0 \to \gamma\gamma$. An NTUPLE is written for events where the χ^2 value for the $p\overline{p}\gamma$ 4-C fit is less than 40.

Further selection criteria, applied in PAW, are:

1. $CL(\gamma p\overline{p}) > 0.05$
2. $CL(\gamma p\overline{p}) > CL(\gamma K^+K^-)$
3. $CL(p\overline{p}\pi^0) < 0.001$
4. $PID_{prob}(p) > 0.02$
5. $PID_{prob}(\overline{p}) > 0.02$
6. $E_{BSC}^{max} < 0.8$
7. $\cos\theta_{max}^{op} < 0.85$

Requirement 3 is necessary for suppressing the abundant background from $J/\psi \to p\overline{p}\pi^0$. Requirement 6 eliminates neutral clusters with more than 80% of the γ energy is in one BSC layer, and requirement 7 is a cut on the minimum opening angle between the charged tracks and the photon, which suppresses γ's that are $\overline{p}$ annihilation products.

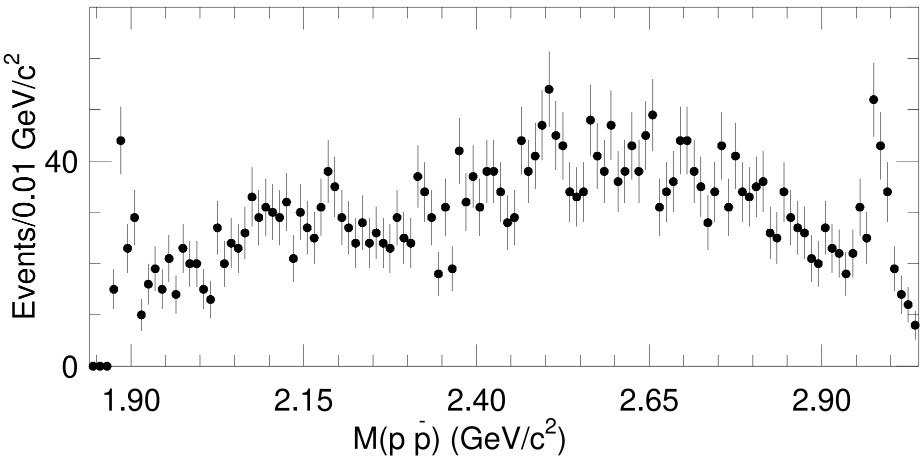

FIG. 1. The $p\overline{p}$ invariant mass distribution from a sample of $J/\psi \to \gamma p\overline{p}$-enriched decays.

Figure 1 shows the $p\overline{p}$ invariant mass distribution for the remaining events. This distribution has a very distinct η_C peak and a narrow peak at the $p\overline{p}$ mass threshold. There is another peak at $M(p\overline{p}) \simeq 2.5$ GeV, but since this is of marginal ($\sim 3.5\sigma$) significance, we defer this for future studies.

III. DETERMINING THE η_C YIELD

Figure 2 shows the results of a fit to the η_C region of the $p\overline{p}$ mass distribution. For this fit, We represent the η_C by a Breit-Wigner function with total width and peak position that are allowed to vary. The background is represented by the functional form

$$f_{bkg} = A_0(\delta^{1/2} + A_1\delta^{3/2} + A_2\delta^{5/2}), \tag{1}$$

where $\delta \equiv M_{J/\psi} - 0.05\ GeV - M_{p\overline{p}}$, is the difference between the nominal maximum and measured $p\overline{p}$ mass (taking into account the $E_\gamma > 0.05$ GeV requirement). The fitting function is convolved with a resolution Gaussian of width $\sigma = 10$ MeV. This is determined by inflating the MC resolution of 8.5 MeV by 20% [2].

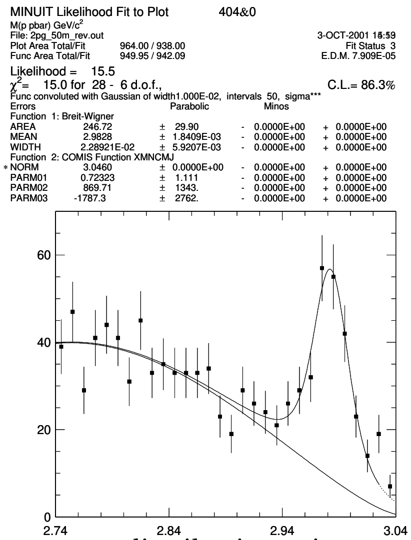

FIG. 2. A fit to the $p\overline{p}$ invariant mass distribution using a resolution-broadened Breit Wigner function for the η_C and a phase-space-like background function described in the text. The region above 3.02 GeV/c^2 is excluded from the fit.

The fit gives an η_C yield of 246.7 ± 53.5 events at a mass of 2983.0 ± 1.8 MeV, and a width of $\Gamma = 22.9 \pm 5.9$ MeV. The mass is 1.2σ higher than the PDG2000 values of 2979.8 ± 1.8 MeV and the width is 1.3σ higher than the PDG2000 value of $13.8^{+3.8}_{-3.2}$ MeV [3]. A MC simulation indicates that the experimental acceptance is 0.28. With this and the nominal number of 50M J/ψ events, we determine a product of branching fractions:

$$\mathcal{B}(J/\psi \to \gamma\eta_C)\mathcal{B}(\eta_C \to p\overline{p}) = (1.8 \pm 0.4) \times 10^{-5}$$

(statistical error only), which is in good agreement with the PDG value of $(1.6 \pm 0.7) \times 10^{-5}$ [3]. (We present this result only as an indication that the results are reasonable. A measurement of the product of branching fractions would require much more careful attention to the background shapes, etc.)

These results indicate that the BESII J/ψ data are of high quality, γ, proton and antiproton track parameters are reliably measured, and our analysis procedure is reasonable.

IV. THE STRUCTURE NEAR THE $p\overline{p}$ MASS THRESHOLD

A. Is the signal real?

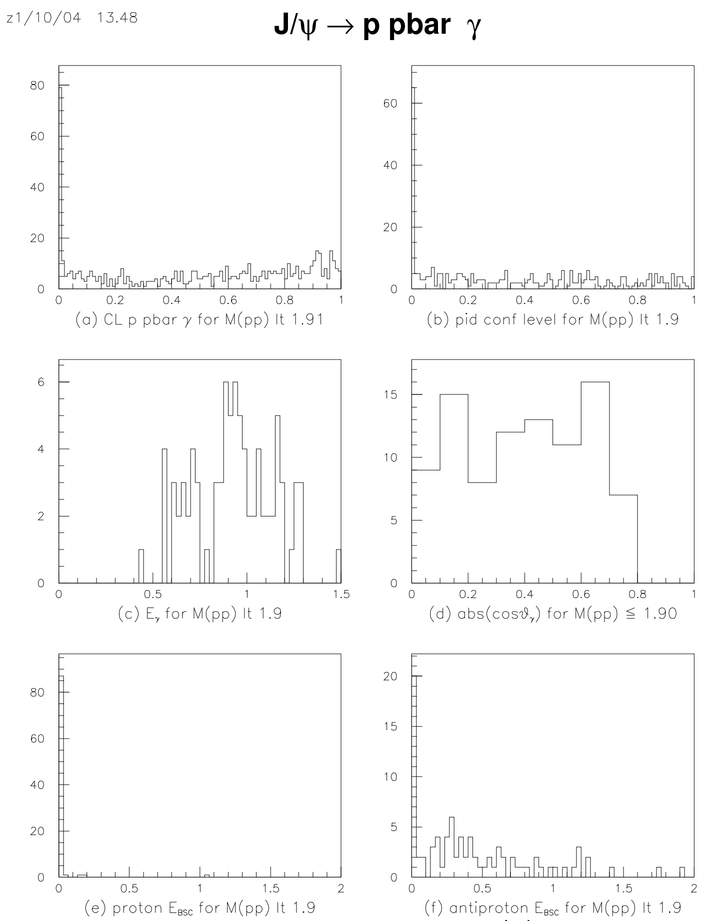

FIG. 3. Distributions for events with $M_{p\overline{p}} < 1.91$ GeV: **(a)** the $\gamma p\overline{p}$ confidence level with the requirement $CL(\gamma p\overline{p}) > 0.05$ relaxed; **(b)** the p and $\overline{p}$ pid confidence level with the pid requirements relaxed; **(c)** the measured γ energies; **(d)** the measured $|\cos\theta_\gamma|$ values; **(e)** the BSC energies for the proton; and **(f)** the BSC energies for the antiproton.

We did some simple checks to demonstrate that the low-mass $p\overline{p}$ peak is not an instrumental effect. Figures 3(a) through (f) show various distributions for events with $M_{p\overline{p}} < 1.9$ GeV.

1. Is some other process fooling the 4-C fit?

Figure 3(a) shows the distribution of $CL(\gamma p\overline{p})$, the 4-C fit confidence level for these events with the $CL > 0.05$ requirement (cut 1) relaxed. Aside from the first bin, which is eliminated by the CL cut, this distribution looks reasonably flat. Figure 3(b) shows the distribution for the proton particle identification probabilities for the tracks in these events (here pid requirements 4 and 5 are relaxed). These distributions are also reasonably flat and show no peculiar behavior. The pid distributions for tagged samples protons and antiprotons are shown in Fig. 4(a) and (b), which verify that these distributions are as expected.

2. Is the peak due to a QED-type background?

One concern is that the peak we see is somehow manufactured by a QED process such as $e^+e^- \to \gamma\gamma$ where one γ converts in the beam pipe and somehow fools the pid and 4-C fit. In this case, the input γ energy would be $E_\gamma = 1.548$ GeV, which is subsequently pulled down by the fit to $E_\gamma \simeq 1.0$ GeV. Figure 3(c) shows the distribution of *measured* γ energies for selected events. Here it can be seen that the measured energies are rather symmetrically distributed around $E_\gamma \simeq 1.0$ GeV with an rms spread of ~ 230 MeV, as expected for the BSC. There is no evidence for a skewing to higher energy values as would be expected for backgrounds that originate from the $e^+e^- \to \gamma\gamma$ process.

Another possible background might be some type of initial-state radiation process. In this case, it would be expected that the γ directions would be concentrated near the beam directions. Figure 3(d)) shows the $|\cos\theta_\gamma|$ distribution for selected events. This distribution shows no strong preference for forward and backward angles. Further evidence against ISR processes is provided by the absence of any evidence for this state in the BES-I $\psi(2S)$ data, as discussed in Section IV C, below.

3. Are these really protons and antiprotons?

The protons and antiprotons for the $M_{p\overline{p}} < 1.90$ GeV mass range have momenta around 0.5 GeV/c and range out in the TOF scintillators and do not enter the BSC. The BSC energy distribution for the protons, Fig. 3(e), shows this quite clearly. The BSC response for the stopped antiprotons, shown in Fig. 3(f), is quite different, because annihilation products can deposit energy in the BSC.

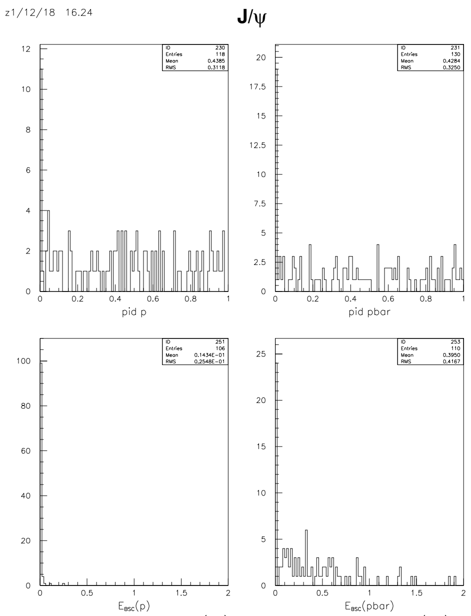

FIG. 4. The pid probabilities for tagged (a) protons and (b) antiprotons in the momentum range $0.4 \leq |\vec{p}| \leq 0.6$ GeV/c from $J/\psi \to \Xi^-\Xi^+$, $\Xi^- \to \Lambda\pi^-$, $\Lambda \to p\pi^-$ (and c.c.) decays. The BSC energy distributions for the same protons (c) and antiprotons (d).

TABLE I. Summary of MC background studies

Channel	$N_{expt'd}$	N_{gen}	N_{sel}	N_{cuts}	$N_{Mp\overline{p}<1.9}$
$\pi^0 p\overline{p}$	55K	80K	25.8K	4.5K	27
$\pi^0\pi^0 p\overline{p}$	≤150K	80K	1.9K	11	0
$\eta p\overline{p}$	105K	40K	568	1	0
$\pi^0\Lambda\overline{\Lambda}$	5K	20K	125	7	0
$\pi^+\pi^-\pi^0 p\overline{p}$	115K	40K	33	1	0
$\Sigma^0\overline{\Sigma^0}$	26K	20K	6	0	0
$\pi^+\pi^- p\overline{p}$	300K	40K	11	3	0
$\Lambda\overline{\Lambda}$	30K	20K	3	0	0

This characteristic BSC response is demonstrated in Figures 4 (c) and (d), which show the BSC using tagged samples of protons and antiprotons with momenta in in the range $0.4 \le p_{\rm lab} \le 0.6$ GeV/c, respectively. These are selected from a clean sample of $J/\psi \to \Xi^-\Xi^+$ decays, where $\Xi^- \to \Lambda\pi^-$, $\Lambda \to p\pi^-$ and $\Xi^+ \to \overline{\Lambda}\pi^+$, $\overline{\Lambda} \to \overline{p}\pi^+$. The BSC response to K^+ and K^- mesons in a similar range selected from $J/\psi \to K^{*\pm}K^{\mp}$ decays and tagged π^+ and π^- from $J/\psi \to \rho\pi$ decays (not shown) show similar BSC responses positive and negative tracks.

B. Background studies

In order to understand the background, we used SOBER to simulate various J/ψ decay processes that produce final states with $p\overline{p}$ pairs. The simulated events are subjected to the same selection and kinematic fitting criteria as are applied to the data. The results of the study are summarized in Table I, where we list the total number of events that are expected in the 50M J/ψ event sample for each decay mode, using PDG branching fractions, together with the numbers of events that were generated, selected, passed all the cuts and have $M_{p\overline{p}} \le 1.90$ GeV/c^2. In all cases, phase-space distributions were used. We find that $J/\psi \to \pi^0 p\overline{p}$ is by far the dominant contributor to the background.

To study this background we selected events with at least two tracks and two γs that satisfied a 4-C fit to the process $J/\psi \to \gamma\gamma p\overline{p}$ and where the fitted $\gamma\gamma$ invariant mass is within ± 35 MeV/c^2 of m_{π^0} to see if there is any similar structure. The mass distribution for $p\overline{p}$ pairs recoiling from the π^0 for these events, shown in Fig. 5(a), shows no prominent feature at low $p\overline{p}$ masses. This distribution is reasonably well represented by a background function of the form given in Eq. 1 above with δ redefined as $\delta \equiv M_{p\overline{p}} - 2m_p$, which is indicated by the curve in the figure.

Figure 5(b) shows the $M_{p\overline{p}}$ distribution for the 80K MC-simulated $J/\psi \to \pi^0 p\overline{p}$ events after the application of the $\pi^0 p\overline{p}$ analysis procedure. The smooth curve in the figure is the result of a fit using f_{bkg} with shape parameters fixed at the values determined from the fit to the data of Fig. 5. The relative normalization for the MC compared to data is 1.44 ± 0.10, in good agreement with expectations based on the PDG $J/\psi \to \pi^0 p\overline{p}$ branching fraction, namely 1.45 ± 0.11 (statistical errors only). Thus, although the MC event sample

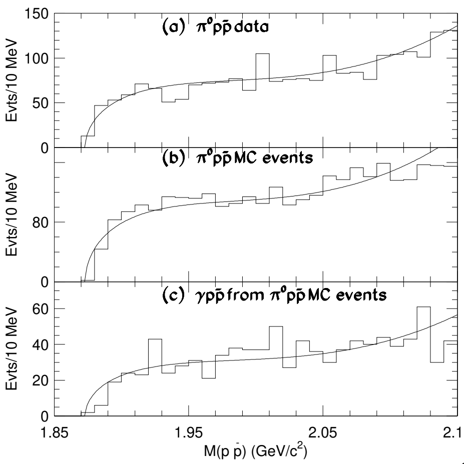

FIG. 5. The $p\overline{p}$ invariant mass distribution recoiling against a π^0 in selected $J/\psi \to \pi^0 p\overline{p}$ events from (a) the data and (b) the $J/\psi \to \pi^0 p\overline{p}$ MC. (c) The $p\overline{p}$ mass distribution for the $J/\psi \to \pi^0 p\overline{p}$ MC events that pass the $\gamma p\overline{p}$ requirements. The fits are described in the text.

is generated with a simple phase-space model, it gives a reasonable representation to the near-threshold region of $p\overline{p}$ mass spectrum; it agrees with the $\pi^0 p\overline{p}$ data in normalization and gives a reasonable reproduction of the shape.

We studied how the $\pi^0 p\overline{p}$ feed-down effects the $\gamma p\overline{p}$ sample by subjecting the MC-simulated $J/\psi \to \pi^0 p\overline{p}$ events to the $\gamma p\overline{p}$ selection procedure. Figure 5(c) shows the resulting $M_{p\overline{p}}$ distribution. The smooth curve is the result of a fit using the f_{bkg} with shape fixed from the $\pi^0 p\overline{p}$ fit. The normalization of this fit relative to that for the $\pi^0 p\overline{p}$-selected MC events is 0.29 ± 0.01 (statistical errors only). The same shape that gives a good representation to the data and MC for the $\pi^0 p\overline{p}$ reproduces the features of the $p\overline{p}$ mass spectrum for the $\pi^0 p\overline{p} \to \gamma p\overline{p}$ feed-down events. There is no artificially induced peaking in the low $p\overline{p}$ invariant mass region. In fact, the background function overestimates the numbers of events near threshold. This is evidence that the structure we see in the $J/\psi \to \gamma p\overline{p}$-enhanced data sample is not due to feed-down from $J/\psi \to \pi^0 p\overline{p}$ events.

As a further check, we examined the low mass region of $p\overline{p}$ mass spectrum for selected $J/\psi \to \pi^0\pi^0 p\overline{p}$ and $\eta p\overline{p}$, $\eta \to \gamma\gamma$ events in the data to see if there were any clustering of events near threshold. Neither channel shows a peaking of events near the mass threshold. Figures6(a) and (b) show the near-threshold $p\overline{p}$ mass distributions for the phase-space MC and data, respectively. The phase-space MC that we used too conclude that $J/\psi \to \eta p\overline{p}$ is not a source of background overestimates the event level near threshold. The same is true for the $\pi^0\pi^0 p\overline{p}$ channel (not shown).

C. Is the structure produced by radiative return?

It has been suggested that the observed structure may have nothing to do with J/ψ decays and is, rather, radiative return to a vector (i.e. $J^{PC} = 1^{--}$) threshold structure that has been observed in the proton's time-like formfactor. If this is the case, the structure should be observed in other BES data samples. We searched for it in the four million $\psi(2S)$ sample.

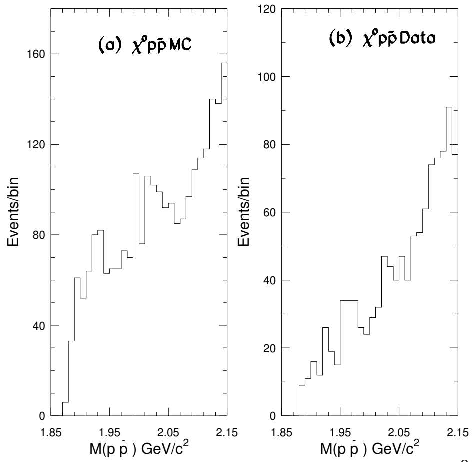

FIG. 6. The $p\overline{p}$ invariant mass distribution recoiling against a π^0 in selected $J/\psi \to \pi^0 p\overline{p}$ events from (a) the $J/\psi \to \eta p\overline{p}$ phase-space MC and (b) the data.

If the observed peak is associated with J/ψ decays, we expect the number of events at the $\psi(2S)$ to scale roughly as

$$n_{\psi(2S)} \sim n_{J/\psi} \times \frac{N_{\psi(2S)}}{N_{J/\psi}} \times 0.14 \simeq \; 0.01 \times n_{J/\psi}, \tag{2}$$

where $n_{J/\psi}$ and $n_{\psi(2S)}$ are the numbers of low-mass events in the J/ψ and $\psi(2S)$ data samples, $N_{J/\psi}$ and $N_{\psi(2S)}$ are the total number of J/ψ and $\psi(2S)$ events, and the final factor of 0.14 comes from the 14% rule.

If, on the other hand, the observed peak is due to radiative return, the scaling goes as [4]

$$n_{\psi(2S)} = n_{J/\psi} \times \frac{\mathcal{L}(\psi(2S))}{\mathcal{L}(J/\psi)} \frac{f(k_{\psi(2S)})}{f(k_{J/\psi})} \frac{M^2_{J/\psi}}{M^2_{\psi(2S)}} = 0.20 \times n_{J/\psi}, \tag{3}$$

where $\mathcal{L}(J/\psi)$ and $\mathcal{L}(\psi(2S))$ are the luminosities (17.7 and 6.0 pb^{-1} for the J/ψ and $\psi(2S)$, respectively), $f(k)$ is the function that describes the energy distribution of ISR photons and $k = 1 - 4m_p^2/s$.

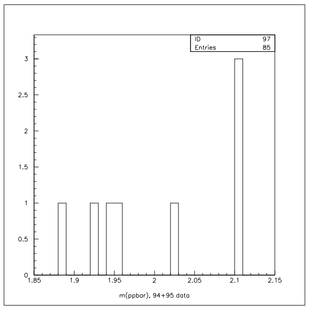

FIG. 7. The low-mass $p\overline{p}$ invariant mass distribution in selected $\psi(2S) \to \gamma p\overline{p}$ events.

Figure 7 shows the near-threshold $p\overline{p}$ mass spectrum for the complete BES-I $\psi(2S)$ data sample, where the event selection is the same as used for J/ψ data, as described above. Here there is only one event with $M_{p\overline{p}} < 1.90$ GeV, where there are ~ 90 events in the J/ψ data. This dearth of events is consistent with the hypothesis that the low-mass peak we see comes from J/ψ decay (Eq. 2) and is inconsistent with radiative-return expectations (Eq. 3).

D. Acceptance

The proton and antiproton detection efficiency of the BES detector falls sharply for particles with three-momenta below 0.4 GeV/c. This produces a mass dependence in the experimental acceptance near $M_{p\overline{p}} \simeq 2m_p$ for $J/\psi \to \gamma p\overline{p}$ and $\pi^0 p\overline{p}$. For both processes, when $M_{p\overline{p}}$ is very near $2m_p$, the p and $\overline{p}$ both have three-momenta very near 0.5 GeV/c and are well detected. For increasing $p\overline{p}$ masses, more asymmetric energy sharing is possible and the acceptance decreases until $M_{p\overline{p}} \simeq 2.0$ GeV/c^2, where it is $\simeq 0.67$ of its value at $M_{p\overline{p}} = 2m_p$. This is shown in Fig. 8, where the data points are acceptance values for each mass bin as determined from MC simulations based on SOBER, with both the γ polar angle distributions and the proton decay angular distribution are generated uniformly. The dashed lines are a fit of two straight lines to the measured acceptance values.

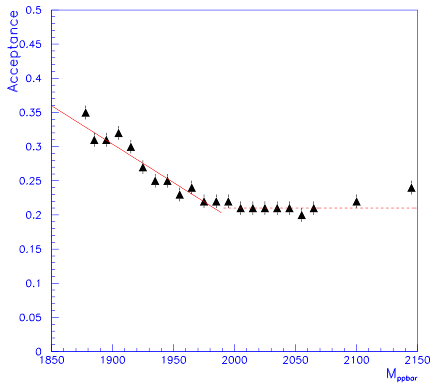

FIG. 8. The variation of the acceptance with $p\overline{p}$ invariant mass for $J/\psi \to \gamma p\overline{p}$ events determined from MC studies using SOBER.

E. Fitting the near-threshold $p\overline{p}$ mass spectrum

Figure 9 shows the low-mass portion of the $p\overline{p}$ invariant mass distribution for the $J/\psi \to \gamma p\overline{p}$-enriched event sample. The acceptance variation is indicated by the dashed curve. We perform a binned, maximum-likelihood fit to this distribution with an acceptance-weighted S-wave Breit Wigner function to represent the signal and f_{bkg}, with shape parameters fixed from the fit to the $p\overline{p}$ masses for the $\pi^0 p\overline{p}$ data sample shown above in Fig. 5(a). The fit, shown as the solid curve in Fig. 9, has $\chi^2/d.o.f. = 28.0/24$.

The results of the fit for the signal Breit Wigner function are: $N_{evts} = 75.0 \pm 13.8$, $M = 1884 \pm 2$ MeV/c^2 , and $\Gamma = 14 \pm 5$ MeV/c^2, where only statistical errors are listed. The fitted f_{bkg} component, shown in the figure as a dotted line, has a normalization that is 0.30 ± 0.03 times that for the fit to the $\pi^0 p\overline{p}$ sample, in good agreement with the MC expectation of 0.29 ± 0.01, (i.e., the ratio of the normalizations from the fits to the MC samples in Figs. 5(c) and (b)).

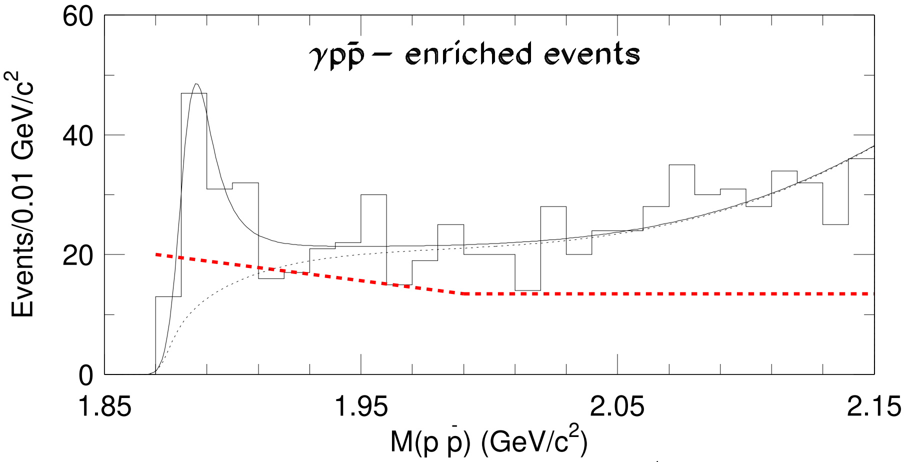

FIG. 9. The fit to $p\overline{p}$ invariant mass distribution for the $J/\psi \to \gamma p\overline{p}$-enriched event sample with an acceptance-weighted S-wave Breit Wigner function used to represent the signal. The solid curve is the result of the fit, the dotted curve is the background component and the dashed curve indicates the acceptance variation as a function of $M_{p\overline{p}}$.

1. *Other fits*

We also fit the near threshold $p\overline{p}$ mass spectrum for the $\gamma p\overline{p}$-enhanced event sample with f_{bkg} only. Figure 10(a) shows the result of a binned likelihood fit using f_{bkg} alone, with the normalization (A_0) and both shape parameters (A_1 and A_2) allowed to float. Figure 10(b) shows the result of a fit with background only with the shape parameters fixed at the results from the fit to the $p\overline{p}\pi^0$ sample described above. Neither fit is an acceptable representation to the data.

We tried to improve the fit by including known particle resonances to represent the low-mass peak. Since the peak is very close to threshold, we restrict ourselves to the case where the p and $\overline{p}$ are in an S-wave. Since, as discussed above, we rule out the possibility of this state being produced by a radiative return process, the S wave assumption implies a $J^{PC} = 0^{-+}$ pseudoscalar state. There are two pseudoscalar resonances listed in the PDG tables in this mass region: the $\eta(1760)$ with $M_{\eta(1760)} = 1.760 \pm 0.011$ GeV and $\Gamma_{\eta(1760)} = 0.060 \pm 0.016$ GeV, and the $\pi(1800)$ with $M_{\pi(1800)} = 1.801 \pm 0.013$ GeV and $\Gamma_{\pi(1800)} = 0.210 \pm 0.015$ GeV. Figure 10(c) shows the result of a fit with a background function with shape fixed from the $p\overline{p}\pi^0$ fit and an S-wave Breit-Wigner function with mass and width fixed at the PDG values for the $\eta(1760)$. This fit has $\chi^2/n_{dof} = 49.1/26$ (CL=0.40%). A fit with the $\pi(1800)$ parameters, shown in Fig. 10(d). is somewhat worse with $\chi^2/n_{dof} = 52.8/26$ (CL=0.15%).

The significance of the signal, determined from $\Sigma = \sqrt{-2\ln(\mathcal{L}(0)/\mathcal{L}_{\max})}$, where $\mathcal{L}_{\max}$ is the likelihood for the nominal signal yield and $\mathcal{L}(0)$ is the value for a fit shown with background only, is $\Sigma = 9.4\sigma$. (Here we use the background-only fit with fixed shape parameters. If we compare to the background-only fit with free shape parameters, the significance is 8.0σ.)

Although the fits that includes the $\eta(1760)$ and $\pi(1800)$ (Fig. 10(c) and (d)) give χ^2 give marginally acceptable confidence levels of of 0.40% and 0.15%, respectively, for the mass range up to 2.15 GeV/c^2, neither fit reproduces the features of the low-mass region as well

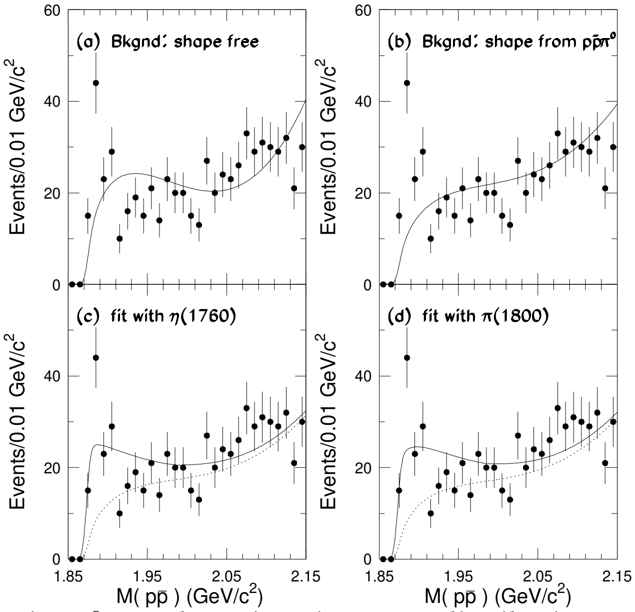

FIG. 10. Results of various fits to the $p\overline{p}$ invariant mass distribution near the $p\overline{p}$ mass threshold. The fits include: (a) background only with shape parameters free; (b) background only with a shape determined from the fit to the $p\overline{p}\pi^0$ sample; (c) an S-wave Breit-Wigner function with mass and width from the $\eta(1760)$ plus a background with the $p\overline{p}\pi^0$ shape; and (d) same as (c) but with the BW mass and width fixed at the PDG values for the $\pi(1800)$. In all cases, the fitting functions are convolved with a Gaussian resolution function.

the fit of Fig. 9, which has a 25.9% confidence level. To compare the relative significance of the fit with the narrow BW signal to that with the $\eta(1760)$, we repeated the fit with f_{bkg} and the $\eta(1760)$ *plus* an S-wave BW component with mass and width allowed to vary. With this addition, the fitted value of the $\eta(1760)$ normalization becomes zero (and tries to go negative) and the parameters of the added BW and the f_{bkg} normalization are identical to those from the fit shown above in Fig. 9. From a comparison the $\ln \mathcal{L}$ values for the fits that include an $\eta(1760)$ with and without the narrow BW term, we find the narrow state is favored by 4.4σ. Similarly, the narrow state is favored over the $\pi(1800)$ by 4.5σ.

F. Angular distributions

For a pseudoscalar $p\overline{p}$ state, the photon polar angle, θ_γ, is expected to have a $1+\cos^2\theta_\gamma$ distribution and the proton helicity angle, θ_{hel}, which is the angle between the proton and the photon in the $p\overline{p}$ rest frame, should have a flat $\cos\theta_{hel}$ distribution. Figure 11(a) shows the acceptance-variation corrected $\cos\theta_\gamma$ distribution for events with $p\overline{p}$ mass below 1.90 GeV. The solid curve shows the result of a fit for $1+\cos^2\theta_\gamma$ to the $|\cos\theta_\gamma| < 0.8$ region; here $\chi^2/d.o.f. = 4.6/7$. For comparison, a fit to $\sin^2\theta_\gamma$, shown as the dashed line, has $\chi^2/d.o.f. = 19.3/7$. Figure 11(b) shows the acceptance corrected $\cos\theta_{hel}$ distribution for the same events, with a best fit constant value superimposed ($\chi^2/d.o.f. = 6.5/9$). Although the results from fitting the angular distributions are not conclusive, they indicate that the data are consistent with the pseudoscalar hypothesis.

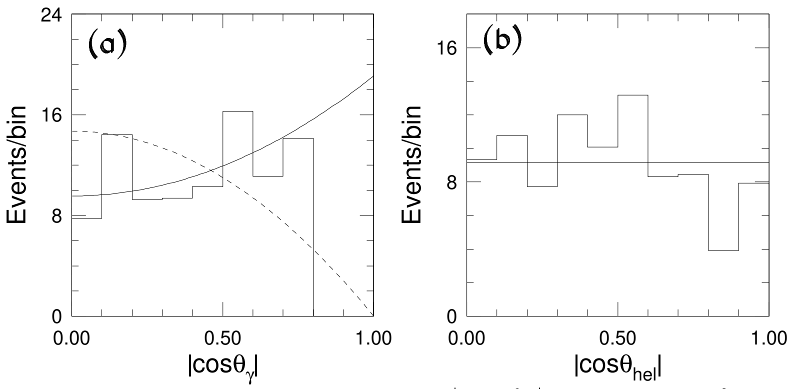

FIG. 11. (a) The acceptance-variation corrected $|\cos\theta_\gamma|$ distribution for the data. The solid curve is a fit for $1+\cos^2\theta_\gamma$ to the $|\cos\theta_\gamma| < 0.7$ region; the dashed curve is a fit for $\sin^2\theta_\gamma$. (b) The acceptance corrected $|\cos\theta_{hel}|$ distribution for the data. The solid curve is the best fit to a single constant.

G. Systematic errors

To determine the systematic errors associated with uncertainties in the fitting procedures, we did the signal fits different ways and recorded the differences. The results are summarized in Table II.

TABLE II. Changes in the number of signal events, δN_{evts}, the peak mass, δM, and peak width, $\delta\Gamma$, for different variations of the fit. Here "slope" refers to the mass dependence of the acceptance and A_1 and A_2 are the shape parameters of f_{bkg}.

Fit variation	$\delta(in\%)$	δM (MeV/c^2)	$\delta\Gamma$ (MeV/c^2)
A_1 & A_2 at MC values	+15.6	-0.5	+1.2
Float A_1 & A_2	+23.1	+1.1	+4.9
resolution×2	-4.0	+0.4	-6.0
resolution→ 0	-0.1	+0.3	+2.5
slope×1.3	-0.8	-0.1	0
slope×0.75	+1.7	0	0
slope→ 0	+4.2	-0.4	-1.0
Extremes	$^{+23.1}_{-4.0}$	$^{+1.1}_{-0.5}$	$^{+4.9}_{-6.0}$

We evaluate the acceptance using SAGEX with different angular distributions and input masses. The results are summarized in Table III.

The acceptance for a $1+\cos^2\theta_\gamma$ distribution is less than for a flat distribution by a factor of $\simeq 0.9$. This is expected for a detector with uniform acceptance in the $|\cos\theta| \leq 0.8$ region. Since the measured angular distributions agree with the $1+\cos^2\theta_\gamma$ expectation, we use this for the acceptance with the difference as the error: 0.29 ± 0.03

For the SAGEX generator, the mass determined from simulated events is several MeV

TABLE III. Results of Monte Carlo simulations for different generated angular distributions and masses. In all cases, 20K events are generated and the input BW width is 20 MeV/c^2.

angular dist	M_{in} (MeV/c^2)	N_{out}/N_{gen}	M_{out} (MeV/c^2)	Γ_{out} (MeV/c^2)
$1+\cos^2\theta_\gamma$	1886.0	0.300	1890.7	17
$1+\cos^2\theta_\gamma$	1880.0	0.292	1888.1	20
$1+\cos^2\theta_\gamma$	1877.0	0.290	1887.0	19
flat	1886.0	0.348	1890.7	16
flat	1880.0	0.335	1888.0	19
flat	1877.0	0.335	1887.3	19

higher than the generated value as can be seen in Table III. We expect that this is because SAGEX does not generate resonances with a proper S-wave shape with a correct threshold dependence but, rather, uses an ordinary Breit Wigner that is truncated at threshold.

The S-wave Breit-Wigner formula for a resonance with mass M_0 and width Γ_0 that we use for fitting is

$$f_{BW} \propto \frac{M_0\Gamma_0(q/q_0)}{(M^2-M_0^2)^2+(M_0\Gamma_0(q/q_0))^2}, \tag{4}$$

where q_0 (q) is the momentum of a daughter particle for the case where the mass value is M_0 (M). *Note that q_0 is not defined for a resonance that peaks below threshold.* In that case we ignore the q dependence of the width term in the denominator.

We made a specialized event generator that produces $p\overline{p}$ states with the S-wave resonance shape using the above formula. The results for the mass determination are plotted in Fig. 12. In this figure the horizontal (vertical) axis is the MC input (output) mass. The dashed lines interpolate the MC results (solid points). The solid horizontal lines indicate the measured mass value and its errors. Here the mass measurement bias for above-threshold input masses is very much reduced, and output masses track the input masses quite well. However, there is a cusp-like behaviour at threshold and a large bias for below-threshold input masses. (This region cannot be investigated with SAGEX, which does not accept below threshold resonance mass inputs.) The vertical dotted lines indicate the possible input values for our $\pm 1\sigma$ measured range. We do not correct the measured value for any possible bias, but include the maximum range of values in the systematic error on the mass.

Another systematic error on the branching fraction is the uncertainty in the number of J/ψ events in the data sample (5%).

1. Branching fraction determination

Using the MC-determined acceptance of 0.29, this corresponds to a product of branching fractions of:

$$\mathcal{B}(J/\psi \to \gamma X_{\overline{N}N(1875)})\mathcal{B}(X_{\overline{N}N(1875)} \to p\overline{p}) = (5.2 \pm 1.0^{+1.8}_{-0.7}) \times 10^{-6}$$

(statistical error only). (Some authors have reported evidence for narrow $\overline{N}N$ states in this mass region [5].)

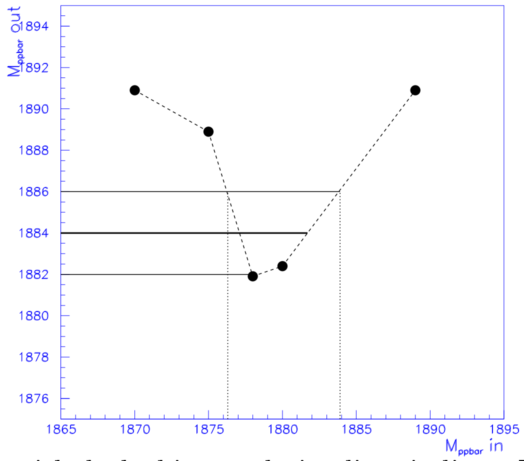

FIG. 12. The solid points with dashed interpolating lines indicate Monte Carlo results for input mass (x-axis) *vs* output mass from the S-wave BW fit. The solid horizontal lines indicate the value of the peak mass from the fit to the data (in Fig. 9).

V. SUMMARY AND DISCUSSION

We observe a narrow structure in the $p\overline{p}$ mass distribution very near the $p\overline{p}$ mass threshold, with a peak mass of $1884 \pm 2 \pm 8$ MeV/c^2 and a narrow width of $14 \pm 5 \pm 5$ MeV/c^2. The statistical significance of the signal is $\geq 8\sigma$. No instrumental or background source for this peak can be found. A similar analysis applied to the same data sample finds a signal for $J/\psi \to \gamma\eta_C$; $\eta_C \to p\overline{p}$ with mass and branching fractions consistent with PDG values. No evidence is found for this structure in the $\psi(2S)$ data sample. This rules out the possibility that the observed state is produced by a radiative return process that is unrelated to J/ψ decays.

Since the p and $\overline{p}$ from this state are very near the $p\overline{p}$ mass threshold, they are most likely in an S-wave. The angular distributions of the final state particles, while not conclusive, are consistent with this expectation. There are no known $J^{PC} = 0^{-+}$ meson resonances in this mass region that have parameters consistent with the results of our fit. We examined the possibility that the structure that we see could be due to the tail of of the $\eta(1760)$, a resonant state reported by the DM2 group in $J/\psi\gamma\rho\rho$ with a branching fraction of $1.3 \pm 0.9 \times 10^-4$. In this scenario, the $\eta(1760) \to p\overline{p}$ branching fraction would have to be comparable to or exceed that for $\eta(1760) \to \rho\rho$ in the kinematically allowed region. A fit to the data that includes both an $\eta(1760)$ and a BW function with free parameters, prefers the narrow state by 4.4σ.

A summary of the masses and product branching fractions for the η_C and the new threshold state are listed in Table IV.

TABLE IV. Preliminary results on masses on the decay branching fractions for particles produced in radiative J/ψ decays that decay to $p\overline{p}$ final states.

Decay Channel	N_{ev}	Mass (MeV/c^2)	Width (MeV/c^2)	$\mathcal{B}(J/\psi \to \gamma\xi)\mathcal{B}(\xi \to p\overline{p})$ (10^{-6})	significance (σ)
$\eta_C \to p\overline{p}$	246.7 ± 53.5	2983.1 ± 1.8	23 ± 6	18 ± 4	many
$X_{\overline{N}N} \to p\overline{p}$	75.0 ± 13.8	$1884 \pm 2 \pm 8$	$14 \pm 5 \pm 5$	$5.2 \pm 1.0^{+1.8}_{-0.7}$	≥ 8

REFERENCES

[1] Copies of transparancies for BES video meeting presentations on Nov. 28, 2001, Dec. 7, 2001 and Jan. 11, 2002 can be accessed at www.phys.hawaii.edu/ solsen/besec/slo.html.

[2] For many different narrow structures, such the $K_S \to \pi^+\pi^-$ and $\phi \to K^+K^-$ peaks, the widths in the data are about 20% broader than those in the MC.

[3] D.E. Groom *et al.* (PDG), Eur. Phys. Journ. **C15**, 1 (2000).

[4] W.M. Dunwoodie, private communication. See also G. Bonneau and F. Martin, Nucl. Phys. **B27**, 381 (1971).

[5] See, for example, A. Antonelli *et al.*, Nucl. Phys. **B517**, 3 (1998), G. Bardin *et al.*, Nucl. Phys. **B411**, 3 (1994), and O.D. Dalkarov *et al.*, Phys. Lett. **B392**, 229 (1997).